








RESEARCH ARTICLE

Microwave dielectric heating affects the in-situ polymerization process of Nylon-6/Ag-NPs hybrid polymer nanocomposite

Yucundo Mendoza Tolentino¹  | Gabriela Yolotzín Romero-Zúñiga²  |
Mónica Aimeé Cenicerros Reyes³  | Pamela Celeste Flores Silva²  |
Ángel Vargas Ramírez²  |
Ernesto Hernández Hernández²  | Pablo González Morones² 

¹Universidad Tecnológica del Valle del Mezquital (UTVM), Ixmiquilpan, Mexico

²Departamento de Materiales Avanzados, Centro de Investigación en Química Aplicada (CIQA), Saltillo, Mexico

³Coordinación del Laboratorio Central de Instrumentación Analítica, Centro de Investigación en Química Aplicada (CIQA), Saltillo, Mexico

Correspondence

Pablo González Morones and Ernesto Hernández Hernández, Departamento de Materiales Avanzados, Centro de Investigación en Química Aplicada, Blvd. Enrique Reyna Hermosillo, Colonia San José de los Cerritos, Saltillo 25294, Mexico.

Email: pablo.gonzalez@ciqa.edu.mx; ernesto.hernandez@ciqa.edu.mx

Funding information

Consejo Nacional de Ciencia y Tecnología (CONACYT), Grant/Award Number: 241960; National Laboratory for Innovation and Development of Lightweight Materials for the Automotive Industry, Grant/Award Number: 321156

Abstract

In this work, the microwave synthesis of Nylon-6 hybrid polymeric nanocomposite (HPNC) was studied by the polymerization of ϵ -caprolactam, 6-aminocaproic acid, and 2% wt of silver nanoparticles (Ag-NPs). It was determined that the dielectric heating (DH) of the Ag-NPs controls the thermal behavior of the HPNCs synthesis and triggers the chemical reaction between Ag-NPs and the Nylon-6 molecules. Such reaction promotes their coating with the polymer and their precipitation, which affects the agitation of the reaction mixture, and results in broader molecular weight distribution and three HPNC populations. Usually, the power output effect in these processes is thermal as it accelerates their heating rate. Still, for HPNCs, higher output reduces the agglomerate size of the Ag-NPs and accelerates their precipitation. At power up to 600 W, the DH of the Ag-NPs causes the explosion of the reaction vials. The antimicrobial activity of the HPNCs against *P. aeruginosa* is almost 100% effective at 180 min of exposure; therefore, this microwave synthesis process is suitable for producing antimicrobial HPNCs.

KEYWORDS

dielectric heating, microwave, nanocomposites, nanoparticles, silver nanoparticles

1 | INTRODUCTION

Many pathogenic microorganisms have developed antibiotic resistance, representing a significant public health problem. For this reason, new bactericidal agents, such as nanoparticles, are being employed and analyzed.^{1–4} These nanoparticles are used to modify surfaces to prevent the growth of microorganisms and the formation of

colonies, which are coated with a compact biofilm that protects them from antibiotics.⁵ The contamination of surfaces in hospitals is a significant problem, as catheters, prostheses, implants, and surgical materials can get contaminated, which causes the majority of hospital infections.^{5,6} To solve this problem, antimicrobial polymeric composites have been developed. For example, polymer nanocomposites with silver nanoparticles (Ag-NPs) can

be used for water sterilization,⁷ manufacture of biomedical devices,⁸ antimicrobial bionanomaterials,⁹ and antimicrobial textiles,^{10,11} among others. These applications are attributed to the biocidal activity of Ag-NPs against 65 types of bacteria, viruses, and fungi, with the advantage that they do not present the problem of microorganism resistance, as occurs with antibiotics.^{1,12–14}

Ag-NPs are blended with polyamides such as Nylon-6 to obtain antimicrobial nanocomposites to manufacture textiles,¹⁵ medical devices,¹⁶ membranes for air filters and water purification,^{17–19} among others. Commonly, these nanocomposites are produced by plasma deposition of Ag-NPs, stabilizing agents, solution spray, and chemical reduction^{18,20–22}; solution mixing²³; melt mixing,²⁴ melt mixing-ultrasound-assisted surface plasma activation²⁵ and melt mixing-silver acetate thermal reduction.^{26,27} However, one of the most critical problems in processing these polymer nanocomposites with Ag-NPs is the dispersion of the nanoparticles in the polymer.^{28,29} This problem can be solved by functionalizing the Ag-NPs with chemical groups similar to the polymer, coating the Ag-NPs with surfactants,³⁰ or grafting the Ag-NPs with polymers compatible with the one they are expected to be mixed.³⁰ The latter option, where the Ag-NPs are chemically grafted with the polymer with which they are mixed, referred to as hybrid polymer nanocomposites (HPNCs), is the best method, as it maximizes the dispersion of the Ag-NPs.²⁸

To produce HPNCs with Ag-NPs, several methods are applied. One of the most widely used consists of performing the polymerization reaction of the monomers in the presence of precursor reagents of Ag-NPs, such as silver nitrate (AgNO_3), where the reagents or polymers are used as reducing agents.^{14,31} However, in these approaches, it is difficult to control the size and shape of Ag-NPs, both critical parameters for their antimicrobial activity.¹³ Microwave (MW) assisted methods are used to control such variables adequately. This type of radiation has been widely used in the synthesis of Ag-NPs where the reducing agents also functionalize or coat the Ag-NPs, which favors their dispersion in the HPNCs.³² The use of MW in the in-situ polymerization processes of Ag-NPs enhances the distribution and adhesion of the Ag-NPs with polymers, such as polystyrene and polymethylmethacrylate.^{33,34} Some authors consider that the improvement in dispersion and adhesion of Ag-NPs with the polymer is attributed to the fast and efficient heating that microwaves produce at a molecular level in each of the reagents³³; thanks to this, the application of MW extends to other methods to produce Ag-NPs, such as curing and deposition of Ag-NPs on textiles.^{10,35}

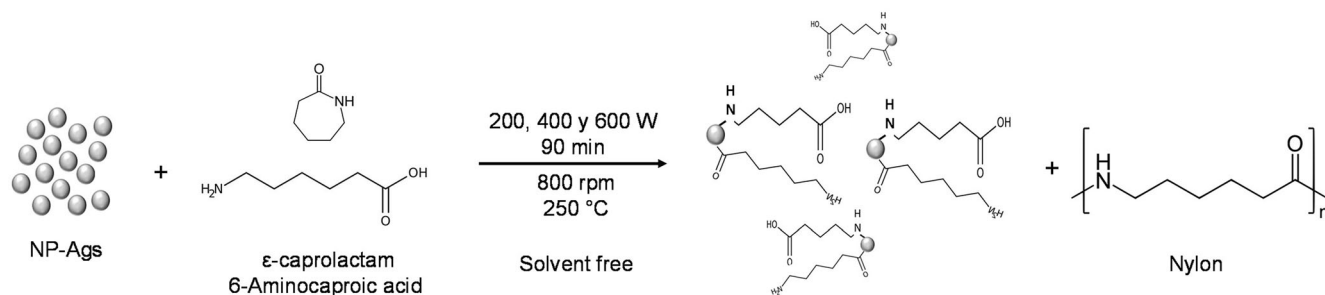
In some of these microwave processes, the effect of both the power and irradiation time of the microwaves³⁶ and the concentration of the Ag-NPs precursor salt³⁷ on the antimicrobial activity of the HPNCs has been demonstrated. For

instance, these variables have been used to control the size, morphology, and concentration of the Ag-NPs in the nanocomposite. Some contributions have examined precursors such as myristate³⁴ and silver nitrate³³ in microwave-assisted in-situ polymerization processes of HPNCs with Ag-NPs. However, using synthesized Ag-NPs produce a better morphology and dispersion of the nanoparticles,³⁸ compared to the nanocomposite obtained without microwaves. Nonetheless, further studies are needed to explain this behavior. Considering the advantages of these microwave-assisted processes, and the fact that remains to be determined and conclusively clarified that the dielectric heating caused by microwaves controls both the physicochemical phenomena that develop during these processes, as well as the final properties of the nanocomposites we aim to study an in-situ polymerization system of Nylon-6 with Ag-NPs, without the use of solvents. The monomers ϵ -caprolactam and 6-aminocaproic acid in solid state (mass polymerization) and Ag-NPs already synthesized were the only materials used to avoid interferences or cross effects generated by more reagents. This study showed that the dielectric heating of the Ag-NPs controls the thermal behavior of the reaction during their heating and promotes the fusion or sintering of some Ag-NPs, their chemical reaction with Nylon-6 molecules, and their agglomeration and precipitation. This affects the molecular weight distribution of the HPNCs, but not their antimicrobial properties, since it reaches 98% at 180 min; meanwhile, the Ag-NPs are present on the surface of the HPNCs. Considering these properties, Nylon-6/Ag-NPs HPNCs have potential applications in the control of the proliferation and propagation of pathogenic microorganisms in materials such as textiles (fabrics and filaments), medical devices, water purification membranes, and in the manufacture of plastic automotive parts that are exposed to users.

2 | EXPERIMENTAL SECTION

2.1 | Materials and reagents

Silver nanoparticles (Ag-NPs) with 99.95% purity, size of 20 to 30 nm, and a density of 10.5 g/cm^3 , coated with polyvinylpyrrolidone (PVP), from Sky Spring Nanomaterials, Inc. were used. The monomers 6-aminocaproic acid and ϵ -caprolactam, reagent grade with a purity of 99%, were purchased from Sigma Aldrich. Reagent-grade solvents with 90% purity were utilized: methyl and ethyl alcohols from Fermont, acetone from CTR Scientific, formic acid from Sigma Aldrich, and distilled deionized water (DDW). For the antibacterial tests, strains of *P. aeruginosa* ATCC #13388 were used as received from



SCHEME 1 The microwave-assisted in-situ polymerization process of the monomers ϵ -caprolactam and 6-aminocaproic acid with pure Ag-NPs (synthesis of HPNCs).

the American Type Culture Collection. This microorganism was grown in Luria Bertani broth (LB), purchased from BD Bioxon, Mexico. Sterile phosphate-buffer saline (PBS) with Tween 80 at 1% was prepared to use in the antibacterial tests according to the ASTM standard E-2180-079 (2012): Standard Test Method for Determining the Activity of Incorporated Antibacterial Agent(s) in Polymeric or Hydrophobic Materials.¹⁷

2.2 | Methods

2.2.1 | Nylon-6 and HPNCs synthesis

The polymerization of pure Nylon-6 and HPNCs with Ag-NPs was carried out in a solvent-free reaction medium (in mass), with the reagents in a solid state, using an Anton Paar Monowave 300 single-mode microwave reactor. The reaction conditions were constant power irradiation of 200, 400, and 600 W for 90 min, with magnetic stirring of 800 rpm, and a reaction temperature of 250°C. For the polymerization of Nylon-6, 20 g of reaction mixture containing the monomers ϵ -caprolactam and 6-aminocaproic acid in an 87:13 (%wt) ratio was used. The monomers were grounded in a mortar until a fine powder was obtained and introduced into a 30 mL borosilicate reaction vial with a magnetic stirrer. Subsequently, a nitrogen stream was passed through this vial for 10 min and sealed with a pressurized septum. For the synthesis of the HPNCs, 20 g of the reaction mixture and Ag-NPs at a 2% wt concentration, based on the weight ratio of ϵ -caprolactam/-6-aminocaproic acid of 87:13, were mixed during the grinding of the monomers (Scheme 1). Each reaction was performed in triplicate to study the reproducibility of these experiments.

2.2.2 | Purification of Nylon-6 and HPNCs

After the polymerization of Nylon-6 and HPNCs with silver, both materials were obtained in solid form and

dissolved in 200 mL of formic acid at room temperature. These solutions were then precipitated by pouring them into a 200 mL ethanol/300 mL DDW solution at a temperature of 85°C with constant stirring. A rotary evaporator at 90°C, 300 rpm, and vacuum pressure was used to extract the formic acid from this dispersion. The obtained paste was re-dispersed in 400 mL of DDW, and again, the rotary evaporator was used to remove the remaining solvent. This operation was performed four times to ensure that all the formic acid was extracted. Finally, the pastes composed of (i) Nylon-6/residual ϵ -caprolactam and (ii) HPNCs with silver/residual ϵ -caprolactam were washed with 500 mL of distilled water at a temperature of 90°C for 30 min. Then, they were filtered at the same temperature to obtain Nylon-6, HPNCs, and residual ϵ -caprolactam dissolved in water as solids.

2.2.3 | Separation of the HPNCs components

10 g of the purified HPNCs were taken and dissolved in 100 mL of formic acid under constant stirring for 6 h at 40°C. A translucent brown solution was obtained and filtered using a polycarbonate membrane with a pore size of 20 nm. The filtered liquid, composed of Nylon-6 and formic acid, was precipitated in DDW. The nanoparticles retained in the filter were again dispersed in 100 mL of formic acid under constant agitation for 6 h at 40°C. This filtration process was performed five times to ensure that the Nylon-6 molecules not chemically bound to the Ag-NPs were separated. The obtained Nylon-6 was precipitated, and the formic acid was extracted using a rotary evaporator, as indicated in the purification of Nylon-6; while the Ag-NPs were dried for 12 h at 80°C.

2.2.4 | Antimicrobial activity of Nylon-6 and HPNCs

Antibacterial properties of Nylon-6 and HPNCs were determined using inoculums of *P. aeruginosa* grown in

LB broth at 37°C for 16 h. Pure Nylon-6 and HPNCs were sterilized using ultraviolet germicidal irradiation by exposure to 254 nm for 30 min. The bacterial suspension was prepared in a sterile solution of LB diluted five times with PBS for a final concentration of 5×10^6 CFU mL⁻¹. 1.25×10^5 CFU mL⁻¹ were placed on the surface of the Nylon-6 and HPNCs films and covered with a sterile cover slip. All samples were incubated for 0, 90, 180, and 360 min at 37°C. The assays were carried out in duplicate in three independent experiments. The bactericide effect was determined by washing each sample with 5 mL of PBS/Tween solution and shaking it in an oscillating platform for 5 min at 88 rpm to detach the bacteria from the film. From each sample, 100 mL of washed solution was placed on LB dishes and incubated for 16 h at 37°C. Antibacterial activity percentage was calculated according to Equation (1),^{39,40} where C_o is the number of bacterial colonies in the control film (pristine Nylon-6), and C is the survival bacterial colonies on the sample films (HPNCs).

$$\text{Antimicrobial activity (\%)} = \frac{C_o - C}{C_o} \times 100 \quad (1)$$

2.2.5 | Characterization techniques

Fourier transform infrared spectroscopy by the attenuated total reflectance method (FTIR-ATR) was used. For this, a Thermo Nicolet infrared spectrophotometer model MAGNA 550 with a gadolinium tip was employed. One hundred scans were collected with 16 cm⁻¹ resolution for all the samples evaluated. To analyze Nylon-6 and HPNCs, films of 1 cm diameter and 100 μm thickness were prepared. For the analysis of Ag-NPs, the gadolinium tip was carefully coated with these NPs. All samples were dried for 12 h at 80°C before the analysis. Raman spectroscopy characterization was performed on a Micro-Raman Horiba Xplora equipment, in a frequency range from 1000 to 400 cm⁻¹, using a 532 nm laser. For thermogravimetric analysis (TGA), TA-Q500 equipment from TA instruments was used. The study conditions were: temperature range from 25 to 600°C, nitrogen atmosphere with a continuous flow of 50 mL/min, and a heating rate of 10°C/min. High-resolution transmission electron microscopy (HRTEM) studies were performed on a TITAN[®] microscope with an accelerating voltage of 100 kV. The evaluation of the samples by scanning electron microscopy (SEM) was performed on a JEOL[®] FE-SEM microscope model JSM-74101 F, with an SEI detector at a voltage of 3.0 kV and 10,000 and 50,000 magnifications. The molecular weight was analyzed by gel permeation chromatography (GPC) using Alliance 2695 equipment with two PLgel columns with a pore size of 5 μm. The sample was diluted in tetrahydrofuran

with 0.05 M trichloroacetic anhydride, and the calibration curve was constructed with polystyrene standards with molecular weights from 2170 to 990, 500 g/mol.

3 | RESULTS AND DISCUSSION

3.1 | In-situ polymerization process

The synthesis process of pure Nylon-6 and its HPNCs with Ag-NPs (Ny-Ag) was evaluated at a 2% wt concentration, an output power of 200, 400, or 600 W at 250°C for 90 min. The thermal and in-situ microwave irradiation behaviors of Ny-Ag 200, 400, and 600 were analyzed. To determine the reproducibility of these experiments and closely study the synthesis process, three identical reactions per power were processed for Nylon-6 and HPNCs. However, the experiments at 600 W could not be analyzed because the reaction vials exploded due to a sudden increase in their pressure and temperature. Figure S1, in the supplementary section, shows the polymerization of Nylon-6 under 200 W output at 250°C for 90 min. The Supplementary section describes the three steps (St1, St2, St3) identified during the synthesis process. However, the most significant change in the temperature behavior was observed in St1; therefore, the first 10 min of the reaction will be analyzed.

Figure 1 shows the temperature behavior for the time or heating rate (HR) of the microwave-assisted polymerizations (MAPs) of Nylon-6 at 200 and 400 W (Figure 1a,b, respectively). The temperature behavior of both powers is very different from each other and heterogeneous. First, at 50°C, HR increases, which is related to the melting of the ε-caprolactam monomer.⁴¹ Then, at 200°C, a temperature behavior reduction is observed due to the beginning of polymerization, which consumes part of the monomer and reduces the heat generated.^{41–43} Finally, a drastic change in temperature occurred. There is an increase above the reaction temperature, considered heating inertia, due to the constant power irradiation mode and the varying composition of the reaction medium between reactants and products.

In the MAPs of the Ny-Ags, the behavior of their HRs is different compared to Nylon-6. For both cases, 200 and 400 W (Figure 2a,b), the temperature behavior is homogeneous and similar among the three polymerization reactions. An increase in the HR is observed between 73.8–74.7°C, which is related to the melting of the monomer, in a temperature range higher than that observed for the MAPs of pure Nylon-6. Furthermore, the thermal effect of the melting and polymerization of the monomers and the heating inertia is lower than the synthesis of Nylon-6. The MAPs of Nylon-6 and Ny-Ags at the

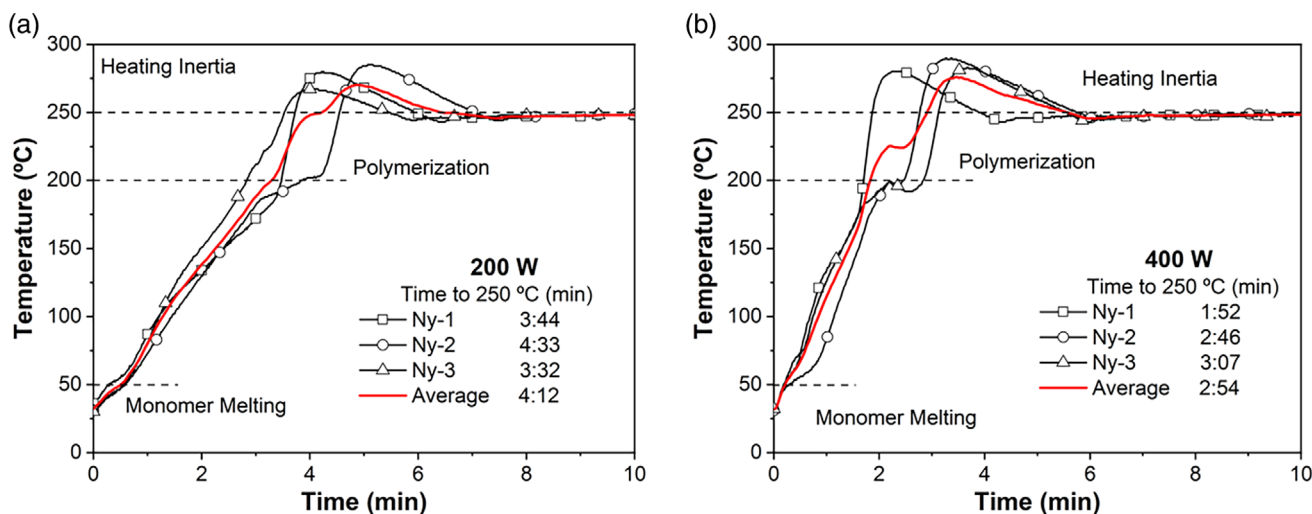


FIGURE 1 In-situ thermal behavior of Nylon-6 MAPs at 200 (a) and 400 W (b) power and the time at which the reaction temperature was reached. [Color figure can be viewed at wileyonlinelibrary.com]

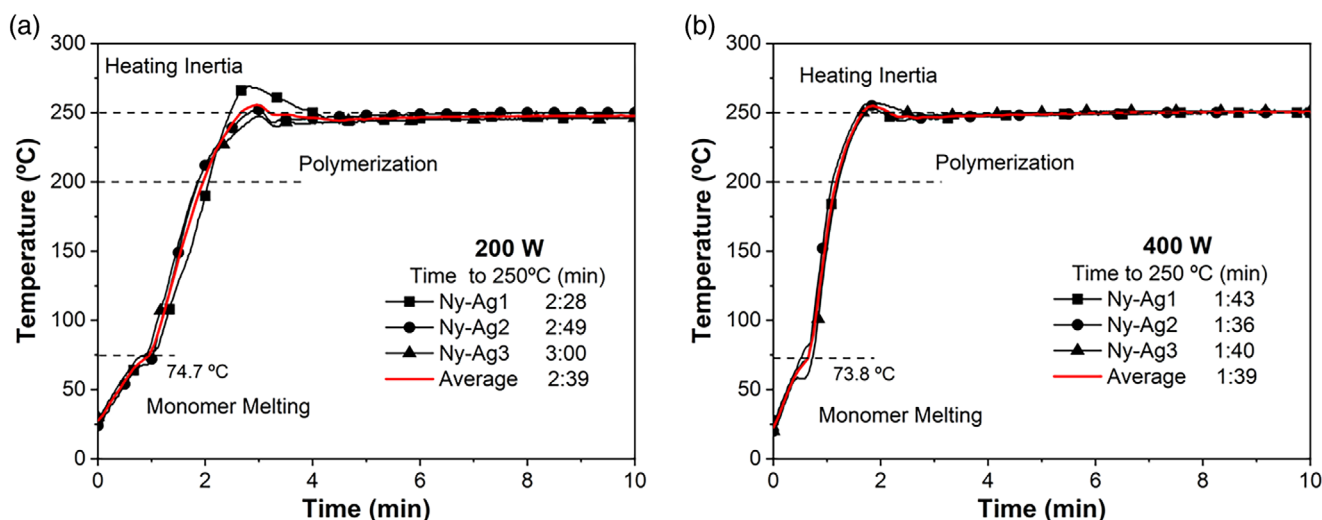


FIGURE 2 In-situ thermal behavior of Ny-Ag MAPs synthesized at 200 (a) and 400 W (b) power and the time at which the reaction temperature was reached. [Color figure can be viewed at wileyonlinelibrary.com]

same power are shown in Figure 3, where the average behavior (calculated with the Origin[®] program) shown in Figures 1 and 2 is plotted.

Figure 3a,b show the thermal behavior of Nylon-6 and Ny-Ag at 200 and 400 W (respectively). The Ny-Ag MAPs reach time at reaction temperature (TRT) faster than the Nylon-6 MAPs, with a reduction in time of 36.98 and 43.10% at 200 and 400 W, respectively. The opposite trend was observed for the HR, where an increase of 58.18 and 42.8% for Ny-Ag MAPs is noted for 200 and 400 W, respectively. These results indicate that the Ag-NPs act as a hot spot by absorbing the microwaves, then transferring their heat to the reaction medium (*ε*-caprolactam/6-aminocaproic acid). Such heat

transfer is so significant that it reduces the perturbations in the HR of MAPs generated by the melting/polymerization of the monomer and the heating inertia. Therefore, the heating of the reaction depends mainly on the heat generated by the Ag-NPs. The effect of power on the MAPs of Nylon-6 and Ny-Ags is shown in Figure S2 of the supplementary data, where it is observed that its effect is purely thermal since the increase in power accelerates the HRs for both cases.

During MAPs of the Ny-Ags, vials reaction showed significant changes in the first 10 min of the reaction, as depicted in Figure 4. For the nanocomposite synthesized at 200 W, the reaction mixture in the vial is black at 0:00 min due to the presence of the Ag-NPs. The melting

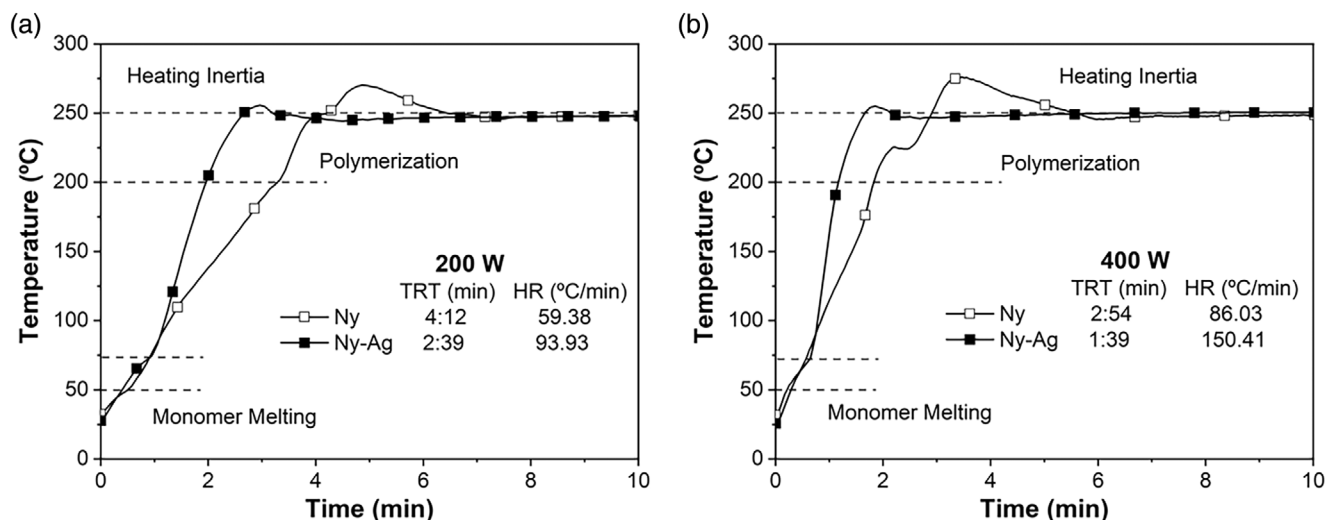


FIGURE 3 Comparison of the in-situ thermal behavior of Ny-Ag and Nylon-6 MAPs synthesized at 200 (a) and 400 W (b) power and the time at which the reaction temperature was reached.

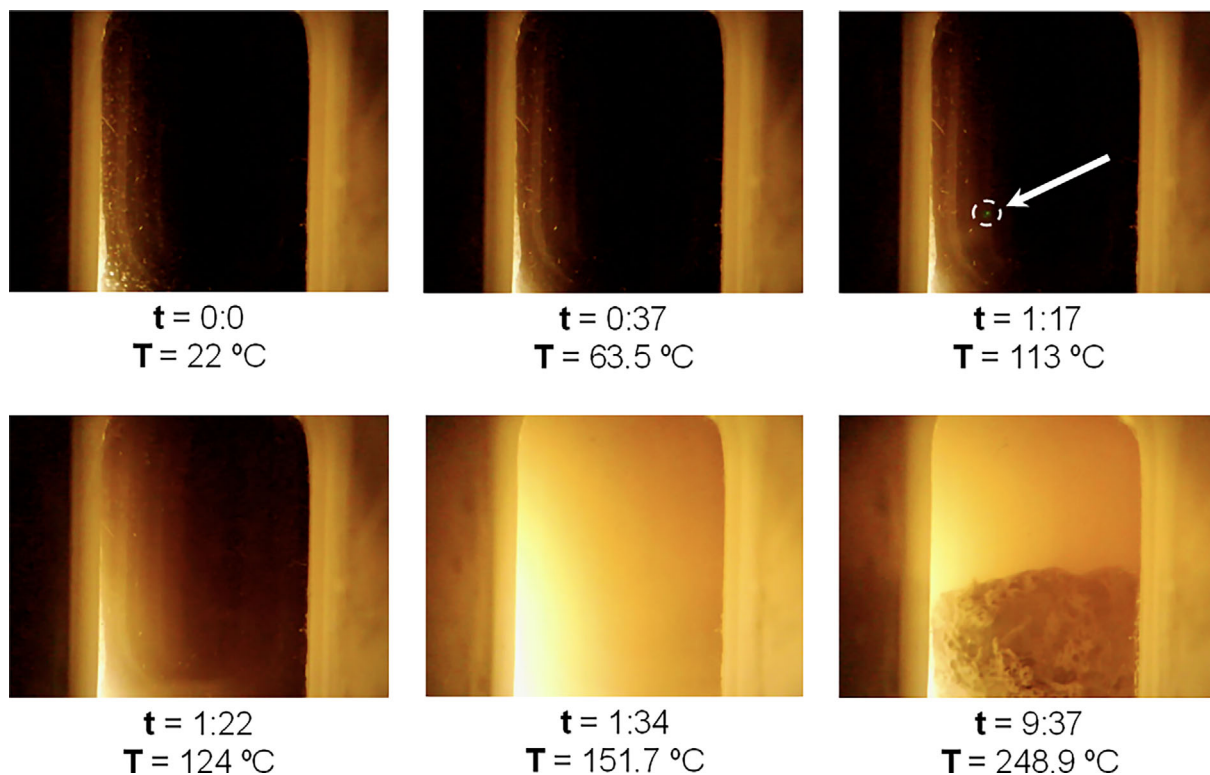


FIGURE 4 Photographs of the reaction vial of the MAPs of the nanocomposite synthesized at 200 W, evidencing the most significant changes in the reaction medium at a given temperature and time. [Color figure can be viewed at wileyonlinelibrary.com]

of the monomer starts at 0:37 min, and at 1:17 min, sparks begin to form in the liquid caused by the heat generated by the Ag-NPs ionizing the reaction medium.⁴⁴ Then, between 1:22 and 1:34 min, and an interval temperature of 124–151°C, the reaction mixture changes its appearance from black to white/translucent, followed by the precipitation of a very large agglomerate at minute

9:37. Similar results were observed in the synthesis of the nanocomposites at 400 W (Figure S3, supplementary information). However, the fusion of the monomer and the formation of the spark started earlier (0:12 min), as well as the agglomeration and precipitation of the Ag-NPs (1:15 to 1:33 min). Moreover, the agglomerates were smaller and looked like powder. Therefore, the results

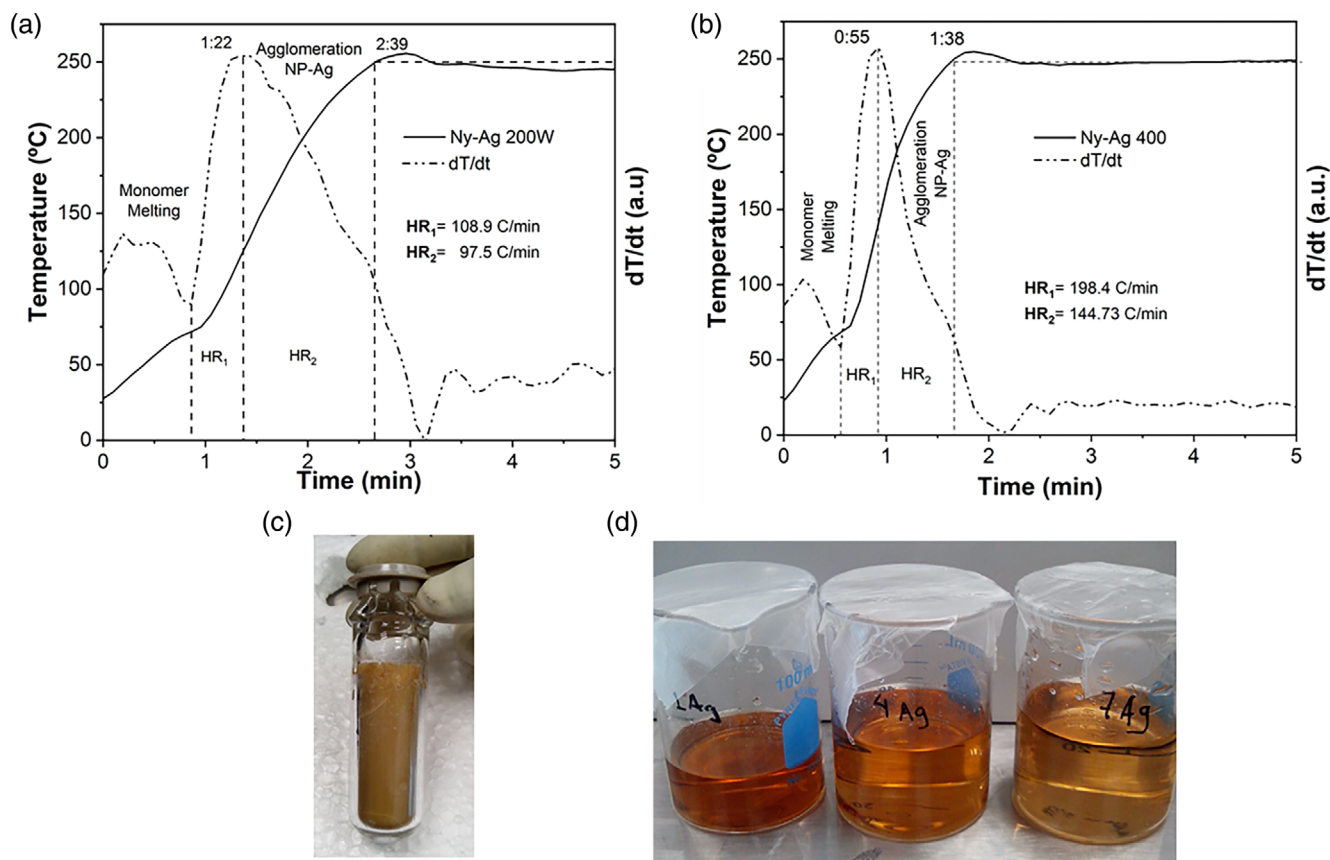


FIGURE 5 Heating rate and derivative of Ny-Ag at 200 and 400 W (a and b); reaction vial after microwave synthesis at 200 W (c), and its three replicates dissolved in formic acid (d). [Color figure can be viewed at wileyonlinelibrary.com]

suggest that the size of the agglomerates and the time at which they precipitate varies according to the power output, that is, at higher power, smaller agglomerates that precipitate in short reaction time are produced, but at lower power, the opposite effect occurs.

Such behavior indicates that, during the Ny-Ags MAPs, the Ag-NPs agglomerate in the liquid state and at a temperature higher than 124°C. This agglomeration can be generated because the Ag-NPs, when heated by microwaves, can reach such a high-temperature point that triggers the fusion or sintering of the Ag-NPs that are in contact or forming agglomerates in the reaction mixture. This heat can also trigger their reaction with the chemical species present in the medium, such as the initiator molecules, the monomer, or the growing Nylon-6 molecules, forming a coating on the Ag-NPs which promotes their agglomeration. Moreover, during the reaction time, there is a viscosity increment that difficult the agitation of the medium and facilitates the fusion/sintering and coating of the Ag-NPs. These results suggest that these types of processes are accelerated or reduced (fusion/sintering and coating) by microwave power. At low power output, there is a longer

100% irradiation time (2:39 min), the agglomerates precipitate slowly, and larger agglomerates are formed.

Meanwhile, there is a short irradiation time (1:39 min) at the high output, and the agglomerates precipitate quickly, reducing their sizes. In both cases (fusion/sintering and coating), the agglomeration of the Ag-NPs should affect both the thermal or HR behavior of the Ny-Ags MAPs and their final properties. Figures 5 A and B show the HR and its derivative for the synthesis of Ny-Ag at 200 and 400 W.

The derivative of the HR of Ny-Ag 200 presents two well-defined peaks (Figure 5a). The first one is related to the melting of the ϵ -caprolactam monomer, and the second peak occurs when the reaction mixture is in the liquid state. The maximum peak is reached at 1:22 min when the agglomeration of the Ag-NPs starts.

Then, the peak decreases until the reaction temperature of 250°C is reached at 2:39 min, so its HR decreases from 108.8 to 97.5°C/min. The synthesis at 400 W (Figure 5b) reveals a similar behavior. However, the changes in the HR occur faster, indicating that the increase in power has a purely thermal effect. In Figure 5c, the reaction vial after the polymerization process at 200 W is observed. No

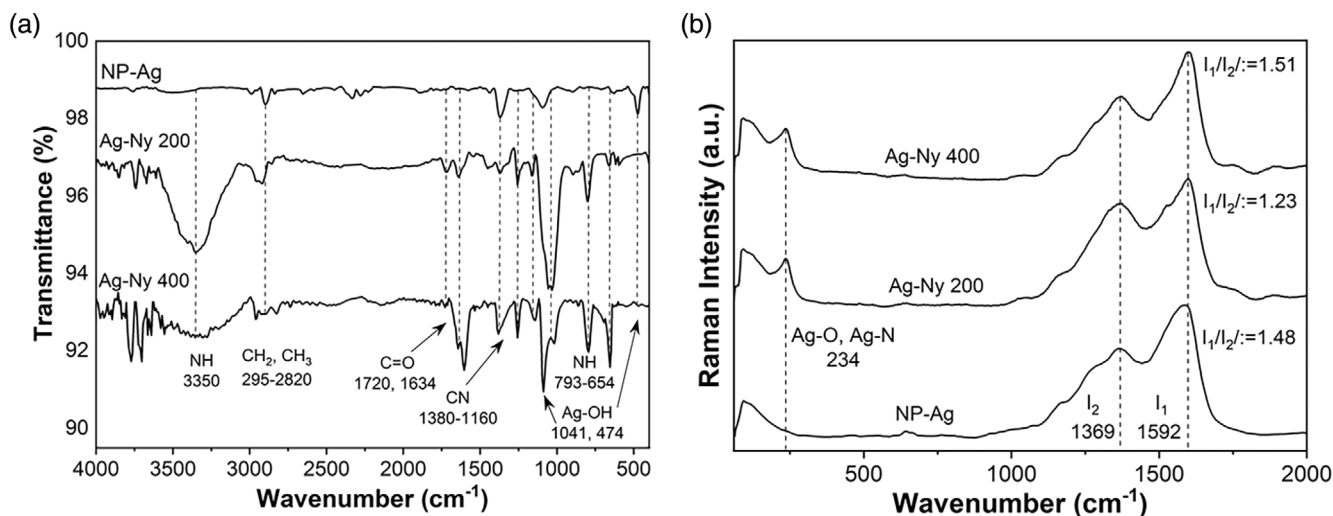


FIGURE 6 FTIR (a) and Raman (b) spectra of silver NPs (Ag-NPs) and silver-nylon nanohybrids synthesized at 200 and 400 W (Ag-Ny 200 and Ag-Ny 400, respectively).

agglomerates are visible at a glance, similarly, when dissolved in formic acid (Figure 5d) for purification. These changes in the HR suggest that the agglomeration caused by fusion/sintering and/or coating of the Ag-NPs reduces their dielectric heating, which has been proved for other NPs and reagents that are heated with microwaves where a change in their physical state and chemical composition modify their dielectric heating.^{41,45} However, since these agglomerates are dissolved or dispersed in formic acid, the coating of Ag-NPs with Nylon-6 molecules is assumed to predominate during the agglomeration process. Ag-NPs were extracted from Ny-Ags and analyzed by FTIR, Raman, TGA, and SEM to inspect this theory, as shown in the following section.

3.2 | Study of the hybridization of Ag-NPs with Nylon-6

The Ag-NPs extracted from the nanocomposites synthesized at 200 and 400 W (labeled as Ag-Ny 200 and Ag-Ny 400, respectively) were characterized by FTIR and Raman spectroscopy. Ag-NPs spectra in Figure 6a shows signals at 3500 cm^{-1} , corresponding to metallic silver (Ag_0), 1041 , and 474 cm^{-1} associated with the vibration/bending of the O—H groups combined with the silver atoms.^{46,47} Ag-Ny 200 and Ag-Ny 400 presented higher intensity peaks than the Ag-NPs spectrum. These peaks are related to the characteristic signals of Nylon-6, such as N—H functional groups at 3350 , 793 , and 654 cm^{-1} ; C=O at 1720 and 1634 cm^{-1} ; and C—N at 1380 , 1255 , and 1160 cm^{-1} . Furthermore, the signal related to Ag-OH at 1041 cm^{-1} showed higher intensity. In the Raman analysis (Figure 6 B) it is observed that all the

samples presented the two characteristic peaks of the Ag-NPs at 1369 (I_2) and 1592 (I_1) cm^{-1} , but their intensities ratio (I_1/I_2) varied. Such variations are generated by the direct binding between the COO-chemical group of the carboxylic acid on the surface of the Ag-NPs.^{48,49} The peak at 234 cm^{-1} , which was only present in Ag-Ny 200 and 400, is attributed to Ag-O and Ag-N stretching, which indicates the formation of a chemical bond between the Ag-NPs surface with the nitrogen of the amino group and the carboxylate group of the COO—.^{49–51}

The FTIR and Raman result demonstrated that Ag-Ny 200 and Ag-Ny 400 chemically reacted with Nylon-6 molecules during the microwave-assisted polymerization process. This hybridization reaction occurs because microwaves dielectrically heat the Ag-NPs and either the functional groups (COO— and NH—) of the 6-aminocaproic acid or the growing Nylon-6 molecules, allowing them to reach the energy levels necessary to produce their chemical reaction and the HPNCs. TGA studies were performed to quantify the amount of Nylon-6 molecules grafting onto Ag-Nys (Figure 7).

The weight loss of Ag-NPs (Figure 7a) about 3.02% wt at 600°C reveals high purity. The highest weight loss occurred between 70 and 350°C (2.64% wt), a characteristic behavior of Ag-NPs coated with polyvinylpyrrolidone (PVP), which is deposited during the synthesis process, as suggested by the manufacturer.⁵² For Nylon-6 synthesized at 200 W (Nylon-6), there is a loss of 93.75% wt before 500°C , which is characteristic of this material. Both nanohybrids (Ag-Ny 200 and 400) showed a thermal behavior similar to Nylon-6, but a weight loss similar to that of Ag-NPs, as it does not exceed 3.2% wt loss. The low concentration of Nylon-6 molecules reacting with the

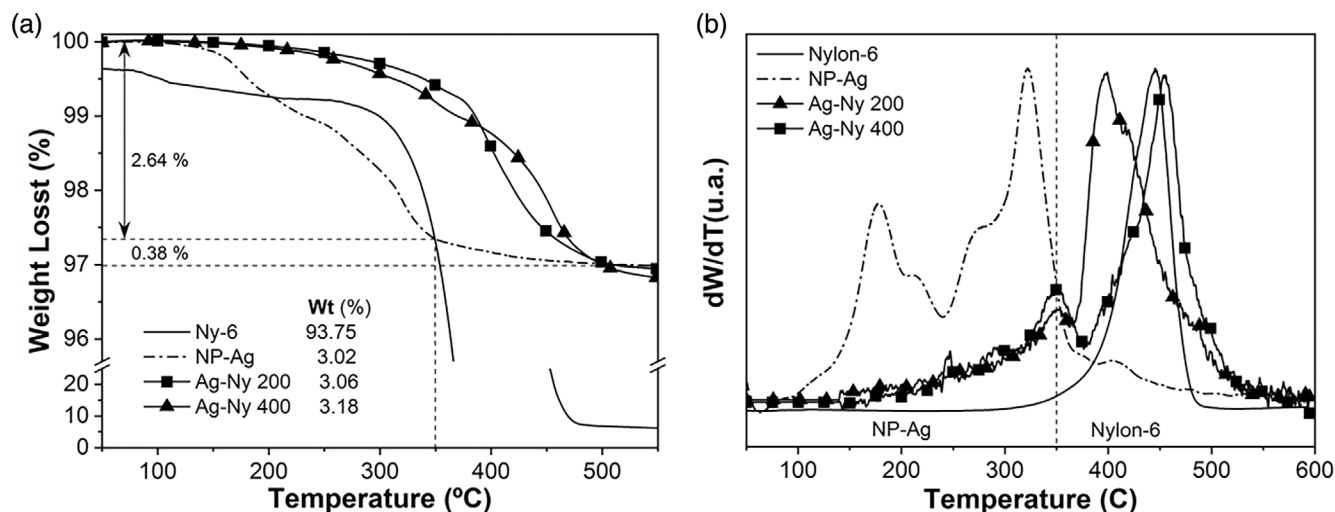


FIGURE 7 TGA thermograms of the nanohybrids (Ag-Ny 200 and 400) and Ag-NPs: percentage weight loss (a) and its derivative (b).

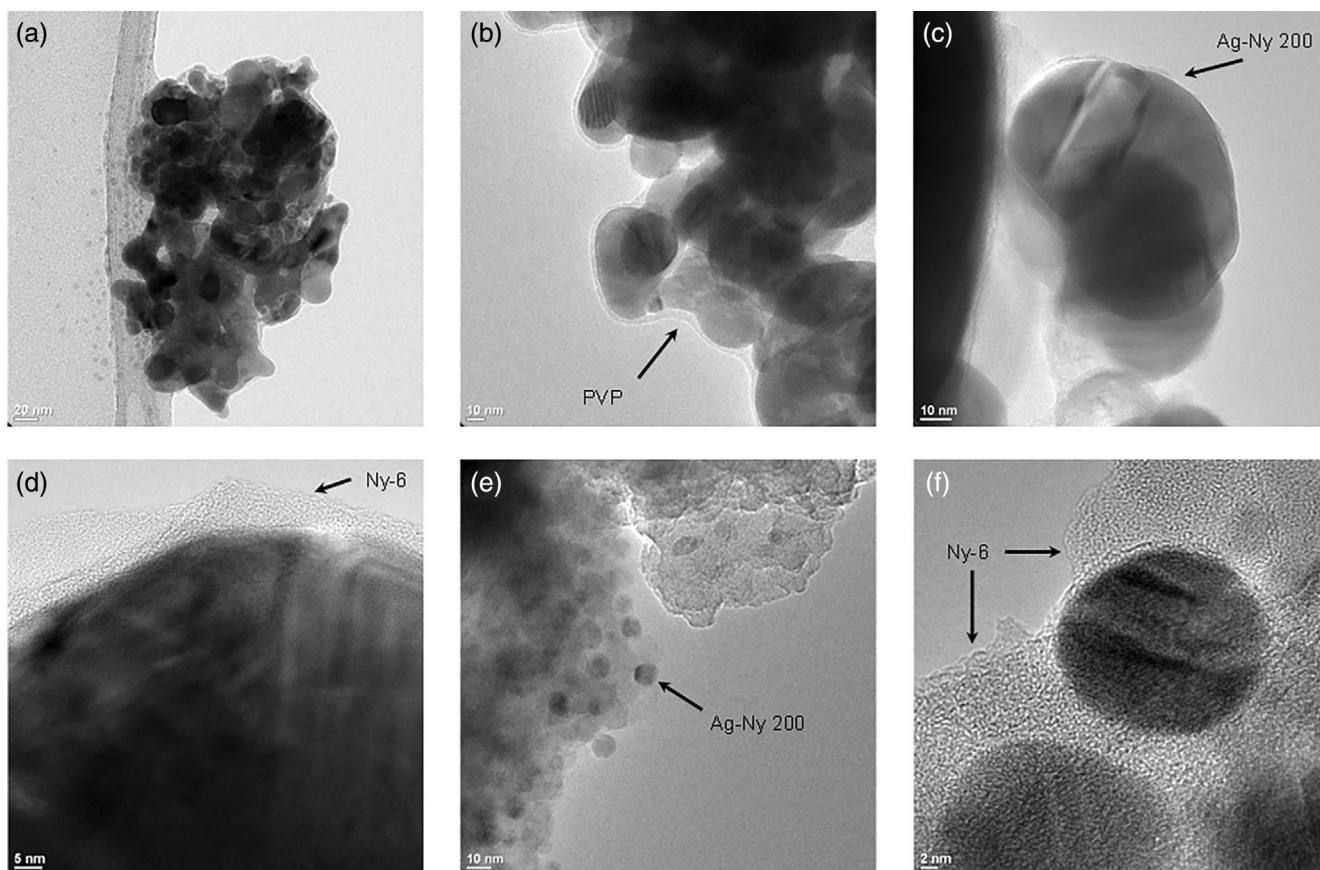


FIGURE 8 TEM micrographs of pure Ag-NPs (a and b) and Ny-Ag 200 nanohybrid (c, d, e, and f) at different magnifications.

surface of Ny-Ag 200 and 400 are attributed to the agglomeration of the Ag-Nys during the first 10 min of reaction since it reduced their exposure and contact with the reactive species during the polymerization process, avoiding the grafting of a higher amount of polymer during the rest of the reaction time. The behavior of the %

weight loss is more evident in the derivative graph (Figure 7b), where it is observed that below 350°C thermal degradation of the trace PVP coating of the Ag-NPs occurs. Still, for Ag-Ny 200 and 400, the thermal degradation occurs above 350°C and is similar to the thermal degradation of Nylon-6.

TABLE 1 EDS chemical analysis of Ag-NPs and Ag-Ny 200.

Element	Ag-NPs (weight %)	Ag-Ny 200 (weight %)
Carbon (C)	1.77	19.99
Nitrogen (N)	0	3.16
Oxygen (O)	0.4	11.89
Silver (Ag)	97.82	64.95

Transmission electron microscopy (TEM) was performed to analyze the Nylon-6 coating grafted on the Ny-Ags (Figure 8). Pure Ag-NP agglomerates with sizes between 9 to 20 nm were observed (Figure 8a). At higher magnifications and with a closer approach (Figure 8b), a PVP coating with a thickness of 1.4 to 5.3 nm was spotted. The chemical characterization of the Ag-NPs was completed by energy-dispersive X-ray spectroscopy (EDS). Figure S3a shows that silver (Ag) is the main component, and carbon (C) and oxygen (O) are present in a lower amount. The quantification of these elements is shown in Table 1, where the weight % concentration of silver is 98. The Ag-Ny 200 nanohybrid had particle sizes from 90 to 300 nm (Figures 8c,d), with an irregular Nylon-6 coating of 5 to 15 nm thickness.

These results confirmed that microwave irradiation increased the size of Ag-NPs by 2 to 10 times compared to their initial size of 20 to 30 nm, due to their fusion/sintering with each other. This fusion/sintering process has been reported in the fabrication of electrodes with Ag-NPs, where output powers of 250 to 1000 W and irradiation times of 20 to 50 s are applied.⁵³ However, Ag-Ny 200 with sizes from 9 to 22 nm were also observed, apparently, they were coated and bonded with Nylon-6 (Figure 8e,f) but were not fused/sintered. With these results, it is considered that the predominant process producing agglomeration and precipitation of Ag-Ny 200 is coating. The chemical characterization by EDS of Ag-Ny 200 is shown in Figure S4b (supplementary section) and the quantification in Table 1, where a considerable increase in the concentration of oxygen, carbon, and nitrogen is observed due to the presence of Nylon-6 in Ny-Ag.

These in-situ studies of the HRs and vials during the first 10 min of reaction, as well as the characterization of the Ag-Ny, extracted from the HPNCs, indicate that microwave radiation produces dielectric heating of the Ag-NPs. This has significant effects on the polymerization process as (i) it controls the heating of the reaction, (ii) activates the surface reactivity of the Ag-NPs and produces their chemical reaction and coating with Nylon-6 (Ag-Ny) molecules, which gives place to (iii) agglomeration and precipitation of the Ag-Ny (Figure 9). Due to these notable effects of dielectric

heating, the final properties of the Ny-Ag nanocomposites were analyzed to determine if they also alter their molecular weight, chemical composition, thermal behavior, and antimicrobial activity.

3.3 | Ny-Ag nanocomposites properties

Figure 10 shows the FTIR-ATR spectra of Nylon-6 MAPs (Figure 10a) and their nanocomposites Ny-Ag (Figure 10b). Both present the characteristic functional groups of Nylon-6 as N—H stretching at 3299–3296 and 3070 cm^{-1} , C=O stretching at 1639–1636 cm^{-1} , N—H in-plane bending at 1543 cm^{-1} , C—N stretching at 1267–1260 cm^{-1} , and out-of-plane bending at 690–687 cm^{-1} . These same functional groups appear in the spectrum of a commercial Nylon-6 from Chemlon[®], which was used as a reference (Ny-Standard). Thus, Ny-Ag is the HPNC of Nylon-6 and Ag-NPs.

The weight losses of the Ny-Ag 200 and 400 and the reference Nylon-6 (Ny-Standard) were calculated by TGA and are shown in Figure 11a. All the samples presented a weight loss between 250 and 600°C. The Ny-Ag lost 97.7%, meanwhile the Ny-Standard 100%. This difference is related to the concentration of the Ag-NP in the nanocomposites (2% wt), while the residual of the Ny-Ag is 2.3%. However, Ny-Ag 200 and 400 presented two significant differences in their thermal behavior compared to Nylon-6, with higher weight loss in the temperature range 290–468°C and 468–550°C.

This thermal behavior was further analyzed with the derivatives of the weight loss (dW/dT) and is presented in Figure 11b. It is observed that all the samples had a slight weight loss between 1.1 to 1.7% at 118°C, which corresponds to the moisture absorbed by the hydrophilic character of the Nylons. Also, the initial thermal degradation temperature (ITDT) for the synthesis of Ny-Ag 200 and 400 is lower (210°C) compared to the Ny-Standard (278°C). The most significant difference is the weight loss at low temperatures (250 to 370°C), which is related to the presence of low molecular weight oligomers, and a second weight loss at high temperatures (470 to 578°C), which originates from high molecular weight (HMW) Nylon-6 molecules. It is also observed that the peak of the derivative representing the maximum rate of weight loss in Ny-Ag 200 and 400 is similar (438°C) but lower than the Ny-Standard of 460°C.

These results indicate that the microwave synthesis of Ny-Ag leads to a heterogenous chain growth since three populations with different thermal stability were identified. To confirm this phenomenon, the molecular weight distribution in weight (M_w) and number (M_n) of the polymerizations of pure Nylon-6 and HPNCs (the polymer

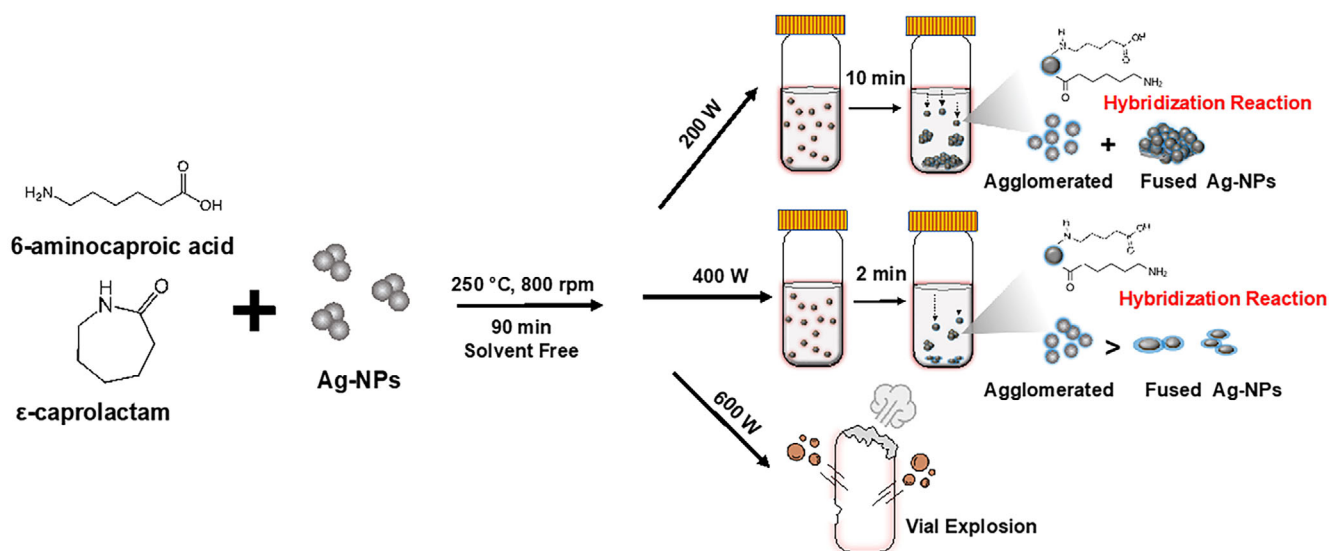


FIGURE 9 Proposed scheme of the microwave-assisted polymerization process of Nylon-6 Ag-NPs HPNCs and their behavior according to the irradiation power. [Color figure can be viewed at wileyonlinelibrary.com]

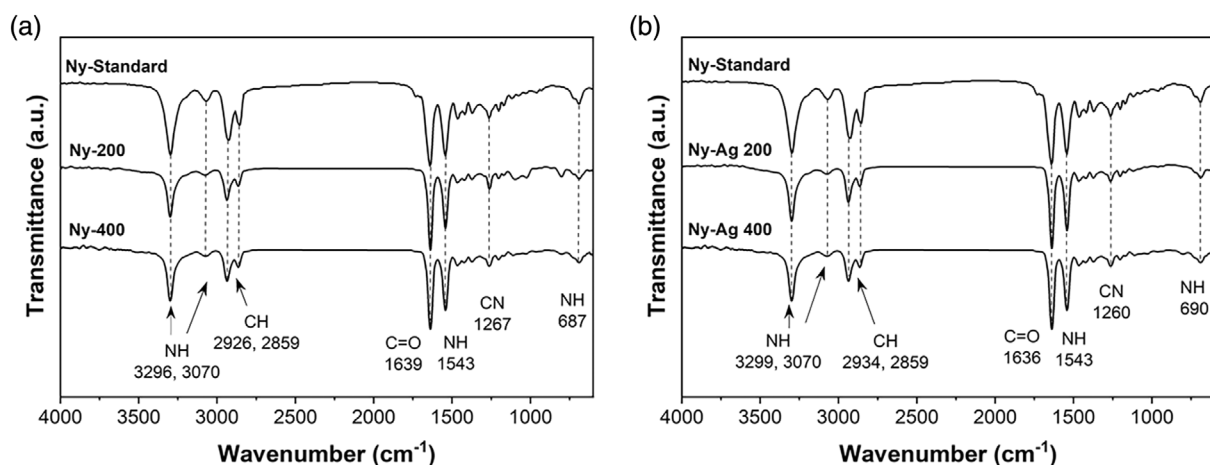


FIGURE 10 FTIR-ATR spectra of Nylon-6 MAPs (a) and HPNCs (b), synthesized at 200 and 400 W power.

that was separated from the Ny-Ag extractions) were assessed by gel permeation chromatography (GPC). The results are shown in Figure 12 and Table 2. The molecular weight distributions of the Ny-Ag 200 and 400 shift toward lower M_w values, compared to Nylon-6 (Ny-200 and 400), but their shape becomes broader involving higher molecular weight population (HMW).

Table 2 shows the M_w and M_n values of all the MAPs. For the synthesis of pure Nylon-6, there are no significant differences in M_w ranging from 3000 to 7000 g/mol; meanwhile, for the HPNCs, there is a substantial difference between 30,000 to 13,800 g/mol. These variations in M_w are caused by the hybridization reaction of the Ny-Ag with the polymer molecules and by their agglomeration. In the first case, the polymerization of Nylon-6 occurs by the ring-opening reactions of ϵ -caprolactam,

and subsequently, its polycondensation and addition reactions, which make the polymer molecules grow. All these reactions are reversible and maintain a chemical equilibrium between the concentration of reactants and products.⁵⁴ As the Ny-Ag are grafted with the polymer molecules, they alter the chemical equilibrium of the reaction, giving rise to populations of different molecular weights (oligomers and HMW).^{42,55} In the second case, when the Ny-Ag agglomerate, the reaction mixture is no longer agitated and homogenized, hindering the encounter between reactive species and generating intermittent growth of the polymer molecules.

The evaluation of the percentage of antimicrobial activity (% AA) with *P. aeruginosa* bacteria, using a variation of the ASTM E2180-07 standard,³⁹ is shown in Figure 13. For the first 90 min, HPNCs Ny-Ag 200 and

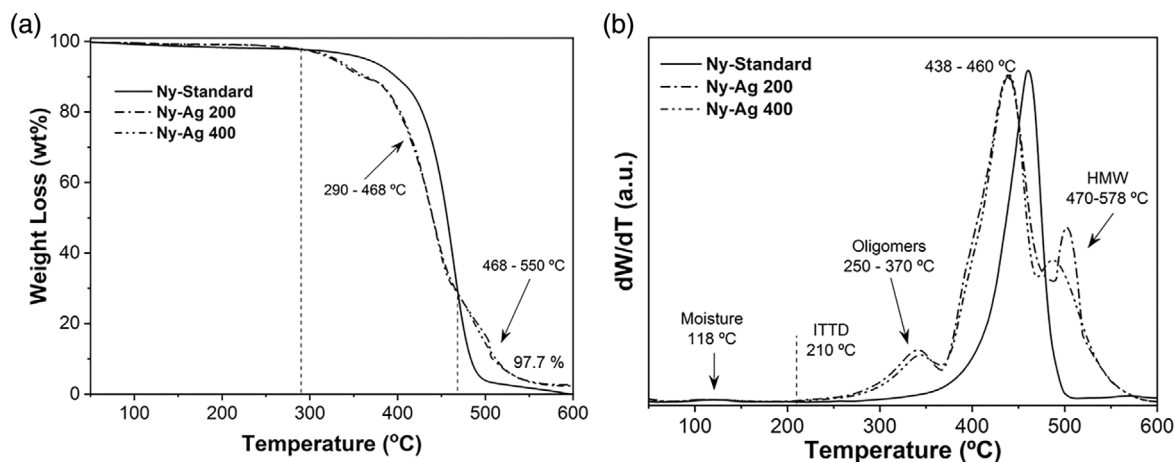


FIGURE 11 TGA curves of weight loss (a) and derivative (b) of Ny-Standard and the nanocomposites (Ny-Ag 200 and 400) synthesized by microwave.

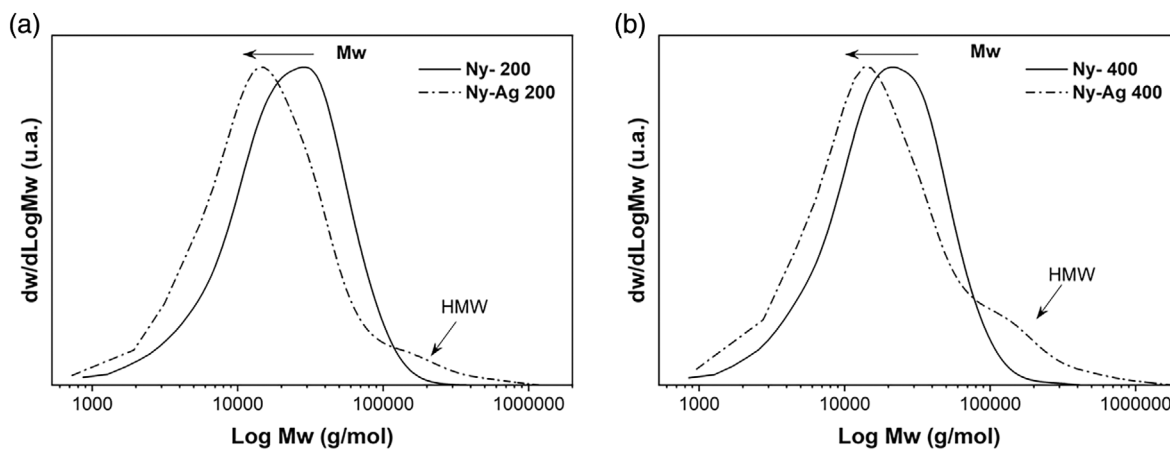


FIGURE 12 Molecular weight distributions of the MAPS of Nylon-6 and Ny-Ag HPNCs at 200 W (a) and 400 W (b) synthesized by microwave.

Nylon-6 synthesis								
	200 W				400 W			
	Ny-1	Ny-2	Ny-3	Average	Ny-1	Ny-2	Ny-3	Average
M_w	31,300	30,100	28,100	29,800	34,000	26,800	29,200	30,000
M_n	12,200	13,600	12,600	12,800	11,300	12,700	12,700	12,200
PD	2.56	2.21	2.23	2.32	2.12	2.11	2.29	2.18
HPNCs Synthesis								
	200 W				400 W			
	Ny-1	Ny-2	Ny-3	Average	Ny-1	Ny-2	Ny-3	Average
M_w	44,400	14,400	21,300	26,700	33,200	19,400	30,300	27,600
M_n	12,200	7300	10,900	10,100	9700	9400	11,200	10,100
PD	3.63	1.97	1.95	2.64	3.42	2.06	2.7	2.73

TABLE 2 Molecular weights in number (M_n) and weight (M_w).

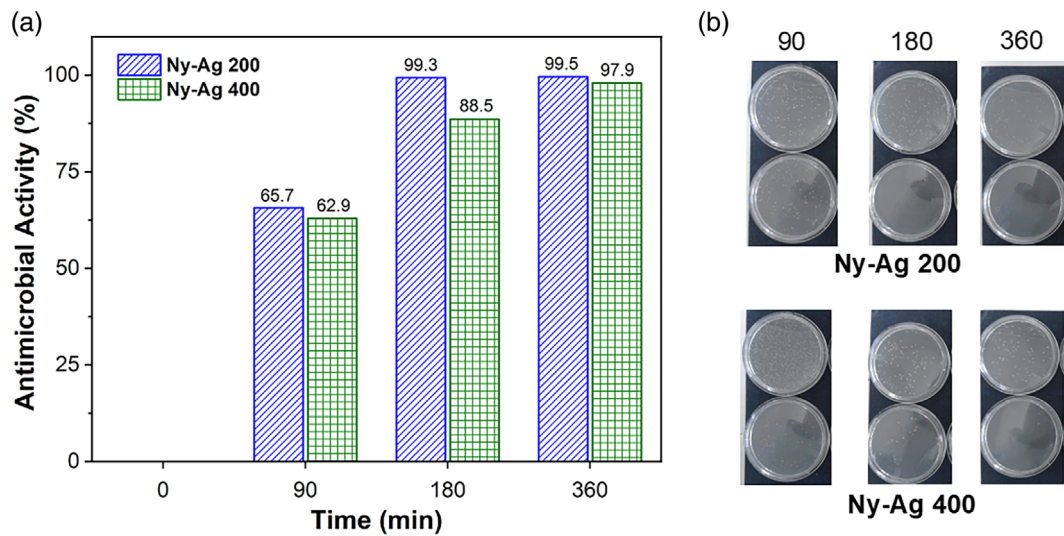


FIGURE 13 HPNCs (Ny-Ag 200 and 400) antimicrobial activity (a) and microbial cultures of *P. aeruginosa* bacteria (b). [Color figure can be viewed at wileyonlinelibrary.com]

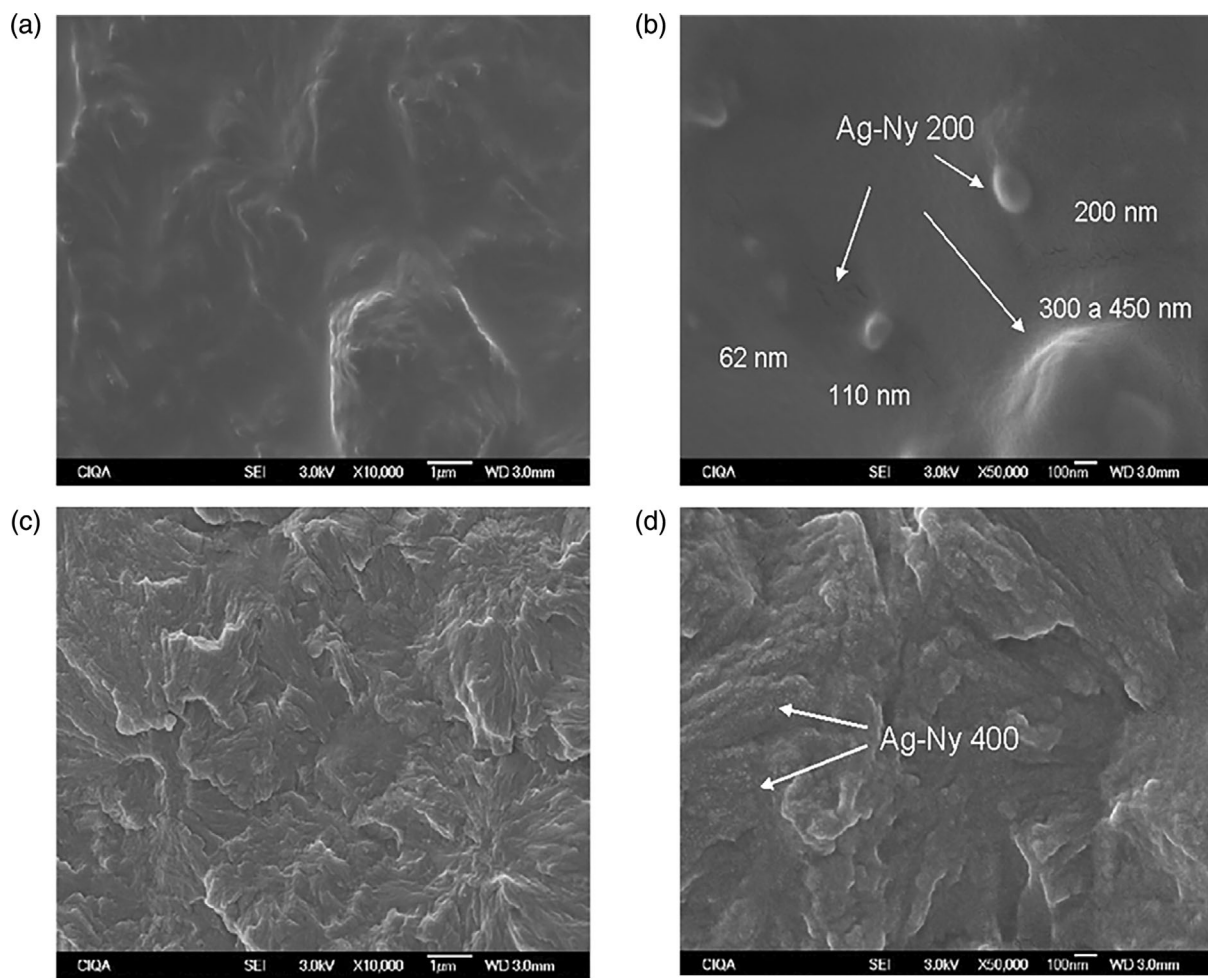


FIGURE 14 SEM micrographs of the fracture surface of Ny-Ag 200 (a and b) and Ny-Ag 400 (c and d) nanocomposites at 10,000 and 50,000 magnifications.

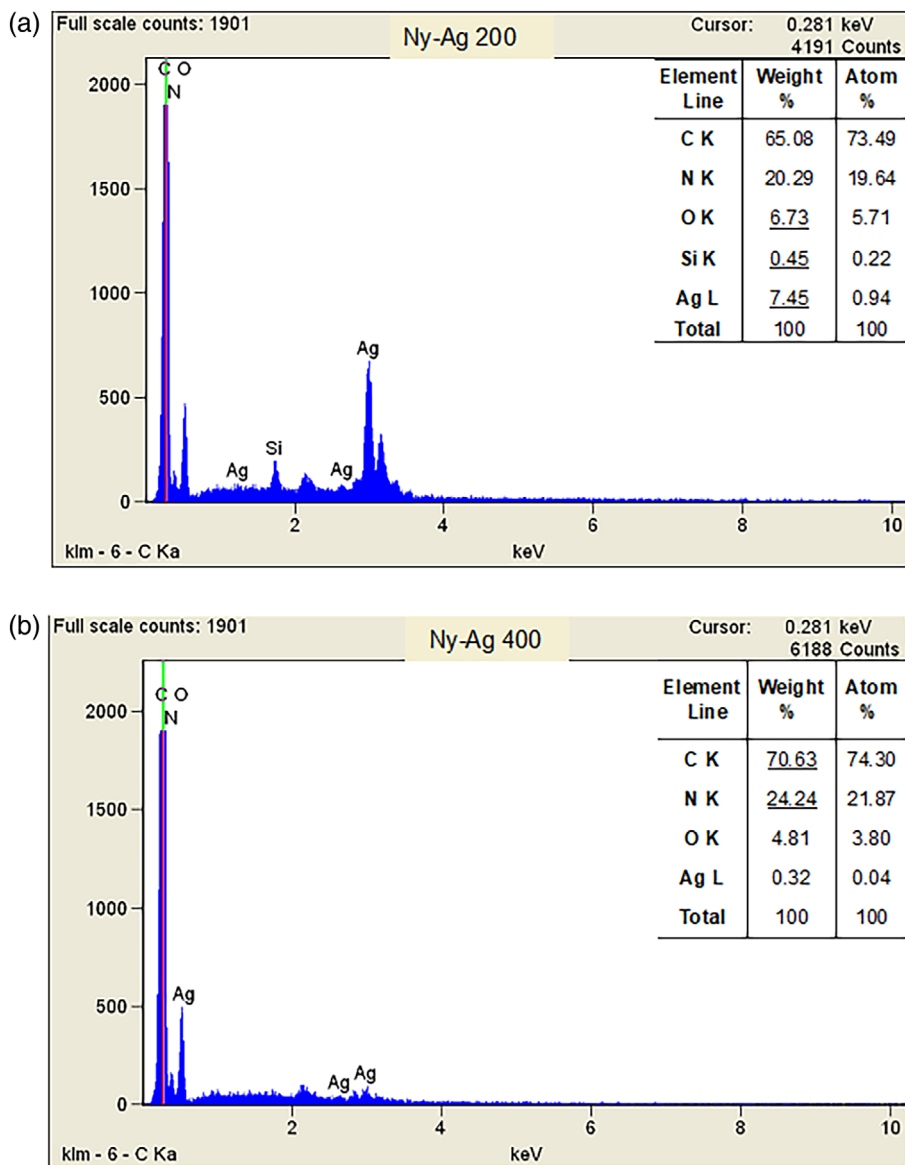


FIGURE 15 EDS chemical analysis of the fracture surface of Ny-Ag 200 (a) and Ny-Ag 400 (b) HPNCs. [Color figure can be viewed at wileyonlinelibrary.com]

Ny-Ag 400 exhibit an antimicrobial activity higher than 60% (Figure 13a). At 180 and 360 min, the antimicrobial activity reaches values close to 100% (Figure 13b). This type of polymer nanocomposites inactivates bacteria by releasing silver ions; however, the release process is affected by the exposure of the Ag-Nys on the surface of the nanocomposites, their oxidation degree, and water exposure. To determine the presence of Ag-Nys on the surface of the nanocomposites (Ny-Ag 200 and 400), they were analyzed by SEM and EDS, as shown in Figures 14 and 15, respectively.

At 10,000 magnifications, both nanocomposites (Figures 14a,c) present a rough surface. At 50,000 (Figure 14b), the Ag-Nys 200 nanohybrids with a size of 200, 110, and 62 nm, as well as some agglomerates with sizes of 300 to 450 nm, were observed. These sizes agree with those previously observed by TEM (Figure 8), which

come from the fusion/sintering of the Ag-NPs. For Ag-Ny 400, at 50,000 magnification (Figure 14d), particles (or agglomerates) with higher contrast are observed. Such particles have sizes from 4.2 to 13.5 nm and may be the Ag-Nys nanohybrids (Figure 3S). As was previously mentioned, during the polymerization process, the Ag-Nys nanohybrids precipitate and formed agglomerates of smaller size compared to the synthesis of Ny-Ag 200. To confirm that these agglomerates are the Ag-Ny, the surface of the HPNCs was analyzed by energy dispersive X-ray spectroscopy (EDS), and the results are shown in Figure 15.

Ny-Ag 200 (Figure 15a) has the highest silver concentration (7.45%); meanwhile, Ny-Ag 400 (Figure 15b) has an Ag concentration of 0.32%. SEM and EDS analyses confirm Ag-Ny on the surface of both HPNCs Ny-Ag 200 and Ny-Ag 400. Ag-Nys are coated with Nylon-6 molecules, improving their compatibility with the matrix,

giving rise to an adequate dispersion in the whole volume of the polymer and the surface of the HPNCs. Additionally, the oxidation of the Ag-Ny was verified by Raman and FTIR spectroscopy studies (Figure 6), which was produced by their hybridization reaction with the Nylon-6 molecules. Furthermore, it is known that Nylon-6 has a hygroscopic nature and can absorb between 2.5 and 3.5% of moisture from the environment.²⁶ These three factors combined stimulate the release of silver ions, allowing these Ny-Ag 200 and 400 HPNCs to exhibit up to 99% antimicrobial activity during the first 180 min of exposure to pathogenic microorganisms.

4 | CONCLUSIONS

This study demonstrates that the DH of Ag-NPs generated by microwaves is the key factor to control both the polymerization process and the final properties of HPNCs. Since the heat and energy of this DH were consumed during the polymerization, a fraction of this heat was dissipated to the reaction medium, which accelerated the overall HR of the reaction, reduced the time at which the reaction temperature was reached and homogenized the thermal behavior of the polymerization reaction. Another part of this energy fused or sintered the small agglomerates of Ag-NPs, increasing their size and producing their hybridization with the Nylon-6 molecules. This hybridization formed a coating on the Ag-NPs, which produced their agglomeration and precipitation, generating low and high-molecular-weight polymer molecules. This also facilitated the dispersion and exposure of the Ag-NPs on the surface of the nanocomposites, which allowed obtaining 99% antimicrobial activity with the *P. aeruginosa* bacteria. In addition, it was found that this DH of the Ag-NPs is controlled by the irradiation power; since, by increasing its value, it increased the DH energy and accelerated the thermal processes, modified the morphology of the Ag-Ny agglomerates, and even produced the explosion and deformation of the reaction vials (Figure S5).

AUTHOR CONTRIBUTIONS

Yucundo Mendoza Tolentino: Writing – review and editing (equal). **Gabriela Yolotzin Romero-Zúñiga:** Investigation (equal); writing – review and editing (equal). **Mónica Aimeé Cenicerros Reyes:** Data curation (equal); writing – review and editing (equal). **Pamela Celeste Flores Silva:** Writing – review and editing (equal). **Ángel Vargas Ramírez:** Investigation (equal); methodology (equal). **Roberto Yáñez-Macias:** Data curation (equal). **Ernesto Hernández Hernández:** Writing – review and editing (equal). **Pablo González Morones:** Resources (lead); writing – original draft (lead); writing – review and editing (equal).

ACKNOWLEDGMENTS

The authors of this work are grateful for the support of the CONACYT project CB-2014-01 No. 241960 and the National Laboratory for Innovation and Development of Lightweight Materials for the Automotive Industry (LANIAUTO) through the CONACYT project 321156. The technical support of Guadalupe Méndez Padilla, Janett Anaíd Valdez Garza, and Carlos Alberto Gallardo Vega is also gratefully acknowledged.

CONFLICT OF INTEREST STATEMENT

The authors declare no conflicts of interest.

CONSENT FOR PUBLICATION


All authors consent to the publication of this manuscript.

DATA AVAILABILITY STATEMENT

Research data are not shared.

ORCID


Yucundo Mendoza Tolentino  <https://orcid.org/0000-0002-1816-8560>

Gabriela Yolotzin Romero-Zúñiga  <https://orcid.org/0000-0001-7728-533X>

Mónica Aimeé Cenicerros Reyes  <https://orcid.org/0000-0002-5106-5782>

Pamela Celeste Flores Silva  <https://orcid.org/0000-0002-8080-5663>

Roberto Yáñez-Macias  <https://orcid.org/0000-0002-9503-2720>

Ernesto Hernández Hernández  <https://orcid.org/0000-0002-7355-566X>

Pablo González Morones  <https://orcid.org/0000-0003-3805-7232>

REFERENCES

- [1] J. R. Morones, J. L. Elechiguerra, A. Camacho, K. Holt, J. B. Kouri, J. T. Ramírez, M. J. Yacaman, *Nanotechnology* **2005**, *16*, 2346.
- [2] M. A. Mahdi, S. R. Yousefi, L. S. Jasim, M. Salavati-Niasari, *Int. J. Hydrogen Energy* **2022**, *47*, 14319.
- [3] S. R. Yousefi, M. Ghanbari, O. Amiri, Z. Marzhoseyni, P. Mehdizadeh, M. Hajizadeh-Oghaz, M. Salavati-Niasari, *J. Am. Ceram. Soc.* **2021**, *104*, 2952.
- [4] S. R. Yousefi, H. A. Alshamsi, O. Amiri, M. Salavati-Niasari, *J. Mol. Liq.* **2021**, *337*, 116405.
- [5] V. Sambhy, M. M. MacBride, B. R. Peterson, A. Sen, *J. Am. Chem. Soc.* **2006**, *128*, 9798.
- [6] H. Palza, *Int. J. Mol. Sci.* **2015**, *16*, 2099.
- [7] S. S. Bag, A. Bora, A. K. Golder, *Polym. Compos.* **2021**, *42*, 6094.
- [8] S. T. Gaballah, H. A. El-Nazer, R. A. Abdel-Monem, M. A. El-Liethy, B. A. Hemdan, S. T. Rabie, *Int. J. Biol. Macromol.* **2019**, *121*, 707.
- [9] M. Hatami, A. Sharifi, H. Karimi-Maleh, H. Agheli, C. Karaman, *Environ. Res.* **2022**, *206*, 112281.

- [10] T. A. Elmaaty, S. M. Ramadan, S. M. N. Eldin, G. Elgamal, *Fibers Polym.* **2018**, *19*, 2317.
- [11] O. Rac-Rumijowska, I. Maliszewska, M. Fiedot-Toboła, I. Karbownik, H. Teterycz, *Polymer* **2019**, *11*, 562.
- [12] M. Ghaffari-Moghaddam, H. Eslahi, *Arab. J. Chem.* **2014**, *7*, 846.
- [13] M. A. Wahab, L. Li, H. Li, A. Abdala, *Nanomaterials* **2021**, *11*, 2870.
- [14] P. Dallas, V. K. Sharma, R. Zboril, *Adv. Colloid Interface Sci.* **2011**, *166*, 119.
- [15] M. E. Yazdanshenas, R. Damerchely, A. S. Rashidi, R. Khajavi, *J. Eng. Fibers Fabr.* **2012**, *7*, 155892501200700108.
- [16] V. Prabhawathi, P. M. Sivakumar, T. Boobalan, C. M. Manohar, M. Doble, *Mater. Sci. Eng., C* **2019**, *94*, 656.
- [17] Z. Jiang, H. Zhang, M. Zhu, D. Lv, J. Yao, R. Xiong, C. Huang, *J. Appl. Polym. Sci.* **2018**, *135*, 45766.
- [18] P. Kleyi, V. Jacobs, C.-K. Na, C. L. Frost, Z. R. Tshentu, N. Torto, *Int. J. Polym. Mater. Polym. Biomater.* **2015**, *64*, 287.
- [19] H. R. Pant, K. T. Pandeya Dr Fau - Nam, W.-I. Nam Kt Fau - Baek, S. T. Baek Wi Fau - Hong, H. Y. Hong St Fau - Kim, H. Y. Kim, *J. Hazard. Mater.*, **2011**, *189*, 465.
- [20] A. I. Ribeiro, M. Modic, U. Cvelbar, G. Dinescu, B. Mitu, A. Nikiforov, C. Leys, I. Kuchakova, A. P. Souto, A. Zille, *AATCC J. Res.* **2020**, *7*, 1.
- [21] M. Montazer, A. Shamei, F. Alimohammadi, *Prog. Org. Coat.* **2012**, *74*, 270.
- [22] S. Sánchez-Valdes, E. Ramírez-Vargas, H. Ortega-Ortiz, L. F. Ramos-deValle, J. Méndez-Nonell, M. Mondragón-Chaparro, G. Neira-Velázquez, I. Yáñez-Flores, D. E. Meza-Rojas, T. Lozano-Ramírez, *J. Appl. Polym. Sci.* **2012**, *123*, 2643.
- [23] H. A. Kim, S. J. Kim, *Fibers Polym.* **2018**, *19*, 211.
- [24] A. D. Erem, G. Ozcan, M. Skrifvars, M. Cakmak, *Fibers Polym.* **2013**, *14*, 1415.
- [25] B. L. España-Sánchez, C. A. Ávila-Orta, M. G. Neira-Velázquez, S. G. Solís-Rosales, P. González -Morones, *MRS Proc.* **2012**, *1479*, 57.
- [26] C. Damm, H. Münstedt, *Appl. Phys. A* **2008**, *91*, 479.
- [27] C. Damm, H. Münstedt, A. Rösch, *Mater. Chem. Phys.* **2008**, *108*, 61.
- [28] J.-B. Zhen, P.-W. Kang, M.-H. Zhao, K.-W. Yang, *Bioconjugate Chem.* **2020**, *31*, 51.
- [29] L. Guo, W. Yuan, Z. Lu, C. M. Li, *Colloids Surf., A* **2013**, *439*, 69.
- [30] U. K. Fatema, M. M. Rahman, M. R. Islam, M. Y. A. Mollah, M. A. B. H. Susan, *J. Colloid Interface Sci.* **2018**, *514*, 648.
- [31] A. Krzywicka, E. Megiel, *Nanomaterials* **2020**, *10*, 2245.
- [32] S. Sharma, K. Virk, K. Sharma, S. K. Bose, V. Kumar, V. Sharma, M. L. Focarete, S. Kalia, *J. Mol. Struct.* **2020**, *1215*, 128298.
- [33] E. H. Alsharaeh, *Materials* **2016**, *9*, 458.
- [34] Y. Wada, T. Kobayashi, H. Yamasaki, T. Sakata, N. Hasegawa, H. Mori, Y. Tsukahara, *Polymer* **2007**, *48*, 1441.
- [35] Q. Wang, L.-M. Barnes, K. I. Maslakov, C. A. Howell, M. J. Illsley, P. Dyer, I. N. Savina, *Mater. Sci. Eng., C* **2021**, *121*, 111859.
- [36] S. Tang, X. Xiao, J. Hu, B. Gao, H. Chen, Z. Zuo, Q. Qi, Z. Peng, J. Wen, D. Zou, *RSC Adv.* **2021**, *11*, 5874.
- [37] A. A.-O. Nicosia, F. Vento, A. A.-O. Pellegrino, V. A.-O. X. Ranc, A. A.-O. Piperno, A. A.-O. Mazzaglia, P. A.-O. Mineo, *J. Nanomater.* **2020**, *10*, 2269.
- [38] E. H. Alsharaeh, A. A. Othman, *Polym. Compos.* **2014**, *35*, 2318.
- [39] B. L. España-Sánchez, C. A. Ávila-Orta, F. Padilla-Vaca, M. G. Neira-Velázquez, P. González-Morones, J. A. Rodríguez-González, E. Hernández-Hernández, Á. Rangel-Serrano, E. D. Barriga-C, L. Yate, R. F. Ziolo, *Plasma Processes Polym.* **2014**, *11*, 353.
- [40] M. Radetić, V. Ilić, V. Vodnik, S. Dimitrijević, P. Jovančić, Z. Šaponjić, J. M. Nedeljković, *Polym. Adv. Technol.* **2008**, *19*, 1816.
- [41] X. Fang, C. D. Simone, E. Vaccaro, S. J. Huang, D. A. Scola, *J. Polym. Sci., Part A: Polym. Chem.* **2002**, *40*, 2264.
- [42] R. Yáñez-Macias, E. Hernandez-Hernandez, C. A. Gallardo-Vega, R. Ledezma-Rodríguez, R. F. Ziolo, Y. Mendoza-Tolentino, S. Fernández-Tavizon, C. A. Avila-Orta, Z. Garcia-Hernandez, P. Gonzalez-Morones, *Polymer* **2019**, *185*, 121946.
- [43] R. Ledezma-Rodríguez, E. H. Hernández, R. Yáñez-Macias, Z. G. Hernández, G. Y. R. Zúñiga, M. G. G. Falcón, C. Gallardo-Vega, P. G. Morones, *J. Appl. Polym. Sci.* **2022**, *139*, 51567.
- [44] V. Tripathi, H. Kumar, A. Agarwal, L. S. Panchakarla, *Beilstein Arch.* **2020**, *11*, 1019.
- [45] K. R. Paton, A. H. Windle, *Carbon* **2008**, *46*, 1935.
- [46] M. H. Baneen, R. M. Baiee, *J. Phys. Conf. Ser.* **2021**, *1999*, 012150.
- [47] A. I. Oje, A. A. Ogwu, M. Mirzaeian, N. Tsendzughul, *J. Electroanal. Chem.* **2018**, *829*, 59.
- [48] M. Kgatshe, O. S. Aremu, L. Katata-Seru, R. Gopane, *J. Nanomater.* **2019**, *2019*, 3501234.
- [49] A. J. Kora, J. Arunachalam, *J. Nanomater.* **2012**, *2012*, 869765.
- [50] A. J. Kora, S. R. Beedu, A. Jayaraman, *Org. Med. Chem. Lett.* **2012**, *2*, 17.
- [51] N. Joshi, N. Jain, A. Pathak, J. Singh, R. Prasad, C. P. Upadhyaya, *J. Sol-Gel Sci. Technol.* **2018**, *86*, 682.
- [52] H. Zhang, G. Zou, L. Liu, H. Tong, Y. Li, H. Bai, A. Wu, *J. Mater. Sci.* **2017**, *52*, 3375.
- [53] T. Chen, H. Yang, S. Bai, Y. Zhang, X. Guo, *R. Soc. Open Sci.*, **2020**, *7*, 191571.
- [54] C. A. Kruissink, G. M. van der Want, A. J. Staverman, *J. Polym. Sci.* **1958**, *30*, 67.
- [55] P. González-Morones, E. Hernández-Hernández, S. Fernández-Tavizón, R. Ledezma-Rodríguez, A. Sáenz-Galindo, G. Cadenas-Pliego, C. A. Ávila-Orta, R. F. Ziolo, *Polymer* **2018**, *146*, 73.

SUPPORTING INFORMATION

Additional supporting information can be found online in the Supporting Information section at the end of this article.

How to cite this article: Y. Mendoza Tolentino, G. Y. Romero-Zúñiga, M. A. Ceniceroy Reyes, P. C. Flores Silva, Á. Vargas Ramírez, R. Yáñez-Macias, E. Hernández Hernández, P. González Morones, *J. Appl. Polym. Sci.* **2023**, *140*(18), e53793. <https://doi.org/10.1002/app.53793>